Effect of Liquid Isothermal Bath Position in Modified Poly(ethylene terephthalate) PET Melt Spinning Process on Properties and Structure of As-Spun and Annealed Filaments

J. F. HOTTER,[1] J. A. CUCULO,[1] P. A. TUCKER,[1] B. K. ANNIS[2]

[1] North Carolina State University, College of Textiles, Raleigh, North Carolina 27695-8301

[2] Oak Ridge National Laboratory, Oak Ridge, Tennessee 37831-6197

Received 31 July 1997; accepted 30 December 1997

ABSTRACT: The ability to produce as-spun poly(ethylene terephthalate) (PET) filaments that possess previously unsurpassed levels of as-spun orientation and tensile properties was achieved through the implementation of a device described as a liquid isothermal bath (LIB). Although much has been published regarding the general effect of the LIB on various properties and structural features, the results of the present study further contribute to the continued development of this unique technology by investigating the positional dependence of the device, as well as the effect of a subsequent annealing process. Characterization methods employed in the present study included birefringence, percent crystallinity, tensile properties, loss tangent temperature dependence, DSC melting behavior, and wide-angle and small-angle X-ray scattering. Strong inferences drawn from the loss tangent temperature dependence indicate that all of the as-spun and annealed LIB filaments possess a more rigid amorphous phase than that present in either the as-spun or annealed no LIB filament and that the extent of rigidness appears to become more profound as the bath is operated at a position more distant from the spinneret. DSC melting endotherms of the as-spun LIB filaments consist of dual overlapping peaks, one component of which is believed to represent the presence of a novel extended chain type of crystalline structure. Application of a simple two phase model allowed for the quantitative evaluation of an amorphous orientation factor, which was found to range, depending on the bath position, from 1.7 to 3.9 times higher in the as-spun LIB filaments than that present in the as-spun no LIB filament. The annealing process was found to play an important role in facilitating the transformation from an as-spun highly oriented and predominantly amorphous structure to a well-defined semicrystalline fibrillar structure. J Appl Polym Sci 69: 2051–2068, 1998

Key words: liquid isothermal bath; poly(ethylene terephthalate); melt spinning; properties; structure; filaments

INTRODUCTION

In a conventional melt spinning process the structure and properties that develop are controlled to a large extent by the manner and magnitude in which threadline deformation occurs during the process of attenuation and cooling. The governing equations (i.e., momentum, energy, and mass balances) describe in detail the manner in which this deformation occurs with respect to the environment and the imposed process conditions. A vari-

Correspondence to: J. Hotter.

Journal of Applied Polymer Science, Vol. 69, 2051–2068 (1998)
 CCC 0021-8995/98/102051-18

ety of process variables exist in conventional melt spinning, such as the extrusion temperature, throughput, draw-down, take-up speed, draw ratio, and so on. Each of these process variables is known to significantly affect the threadline dynamics, as well as the resulting filament structure and properties. However, the undoubtedly numerous studies that have attempted to optimize the combination of all of these variables have yet to yield a process that produces a filament with properties significantly beyond those that could be achieved 25 years ago. From one perspective, this limitation is considered inevitable and is accepted as a consequence of the highly isotropic and entangled nature of the precursor polymer melt. From another perspective, it can be argued that if judicious control, well beyond that present in conventional spinning, can be achieved then it may be possible to go directly from the isotropic melt to a fully oriented as-spun filament that possesses a more extended chain-type structure. Were such a transformation possible, the ultimate expectation of producing, in a single step, a synthetic filament with properties more closely approaching the theoretical limits of strength and stiffness might be closer to realization. However, to achieve such control, the spinning environment will likely require a radical type of threadline perturbation or modification.

Numerous attempts have been made to alter the threadline dynamics of a conventional melt spinning process through modified air quenches.[1–4] While these modified air quenches have altered the dynamics and the resulting filament structure and properties, the changes incurred were relatively small compared to the desired effect. This limited success, however, inspired the investigation of other more radical types of modifications. Possibly the most radical type of modification attempted to date was the introduction of a liquid isothermal bath (LIB) into the path of a developing poly(ethylene terephthalate) (PET) melt spinning threadline. This LIB modified process was shown to be capable of increasing the as-spun filament tenacity and modulus to levels comparable to fully drawn filaments.[5–8] In the present study, the effect of LIB position on the spinning process and the structure and properties of as-spun and annealed PET filaments were examined.

EXPERIMENTAL

Filament Spinning

A high molecular weight PET chip was used to produce all of the as-spun and annealed filament samples. The intrinsic viscosity of the virgin chip was measured in a 60/40 wt % phenol/tetrachloroethane solution and is reported to be 0.97 dL/g. The filament was extruded from a single hole spinneret having an exit diameter of 0.6 mm. Figure 1 shows the experimental setup used in the preparation of as-spun and annealed samples. The take-up speed was fixed at 4000 m/min during the collection of all as-spun filaments. The polymer throughput was held constant to achieve comparable linear densities of approximately 4.5 denier (d) in all of the as-spun filaments.

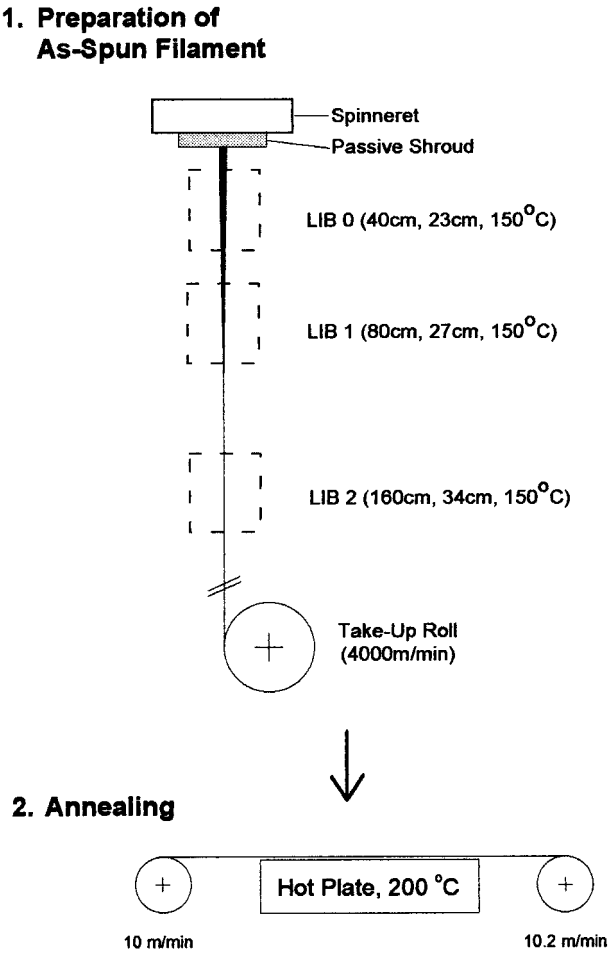

Figure 1 Experimental setup used in the preparation of as-spun and annealed PET filaments produced using a liquid isothermal bath modified spinning process.

Three LIB positions were investigated. These positions were designated as LIB 0, LIB 1, and LIB 2; position 0 was closest to the spinneret and position 2 was farthest from the spinneret. The liquid medium used in this study was 1,2 propanediol. The process variables associated with

operation of the bath are the distance from the spinneret to the bottom of the bath (40, 80, and 160 cm), the depth of the liquid (23, 27, and 34 cm), and the temperature of the liquid (150°C for all cases). The correspondence between LIB position and the value of each of these process variables is shown in Figure 1. In each case, the maximum possible depth of liquid was determined and then maintained during the process of sample collection. Along with the three samples produced using the LIB modified spinning process, a fourth control sample produced from an unperturbed spinning process (no LIB) was also collected. Each of the as-spun samples was subsequently annealed under essentially a fixed length condition by passing the continuous filament across a 30 cm long hot plate using a small pair of low speed rolls. The annealing process imposed a relatively constant exposure time of approximately 1.8 s across the hot plate, which was held at 200°C.

Filament Characterization

Crystallinity

Filament density was experimentally determined using a density gradient column according to ASTM D1505-68. Aqueous sodium bromide solution was used and maintained at 23 ± 0.1°C. Air bubbles were eliminated and wetability improved by centrifuging filament samples in solution prior to placement in the gradient column. Using glass reference beads of known density, an equation describing the linear density gradient within the column could be determined from regression analysis. From this equation the density of the filament samples was calculated from their equilibrium final resting position in the column. The measured density values were then converted to a volume fraction of crystallinity by simply interpolating between the densities of the completely amorphous and completely crystalline phases, as shown in eq. (1).

$$V_c = (\rho - \rho_a)/(\rho_c - \rho_a) \qquad (1)$$

Density values representative of the amorphous (ρ_a) and crystalline (ρ_c) phases were taken as 1.335 and 1.495 g/mL,[9] respectively.

Birefringence

A Jena interference microscope was used to characterize the filament samples. A zenon light source combined with an orange filter provided monochromatic illumination of a 589-nm wavelength. A series of Cargille refractive index liquids were used to arrive at a retardation band displacement suitable for measurement. The mean birefringence (Δn) values were then calculated as follows:

$$\Delta n = n_{\parallel} - n_{\perp} \qquad (2)$$

Use of the interference technique for mean birefringence circumvented the problem associated with dispersion effects that becomes significant at high orders of retardation. Radial birefringence profiles were calculated using the shell model with the aid of an image analysis system.[10,11]

Tensile Properties

Mechanical properties were measured using a table model 1122 Instron tester. Properties to be reported include tenacity, elongation to break, initial modulus, and a stress amplification ratio (SAR). The SAR was calculated as the ratio of the secant modulus at 5% elongation to the initial modulus and is considered to provide a measure of the deviation from linearity that occurs just beyond the yield point. All calculations were performed in accord with ASTM D3822-82. All tests utilized single filaments of 25.4-mm gauge length. A constant rate of extension of 20 mm/min was imposed during all tensile tests. The values reported for each quantity represent the average of seven individual measurements.

Thermal Shrinkage

The measurement of boil-off shrinkage for select as-spun fibers was performed according to ASTM D2102-79. The measurement of free shrinkage at 177°C for select posttreated fibers was performed in accordance with ASTM D885-78. In either case the shrinkage was calculated as follows:

$$\text{shrinkage}\ (\%) = [(I - F)/I] \times 100 \qquad (3)$$

where I is the initial length of the specimen and F the final length of the specimen.

Dynamic Mechanical Analysis

Dynamic mechanical measurements were performed on a Rheovibron model DDVII-C viscoelastometer manufactured by IMASS. In this test the

ends of a 50-d filament bundle are mounted on opposing strain gauges using a gauge length of 20 mm. One end of the bundle is subjected to a sinusoidal tensile strain that results in a displaced sinusoidal stress at the other end of the sample. The phase angle between these two sinusoidal waves is monitored and reported as a tan δ value. The storage modulus, E', in phase with the imposed strain, and the loss modulus, E'', out of phase with the imposed strain, are related through the value of tan δ as follows:

$$\tan \delta = E''/E' \tag{4}$$

The rheovibron was operated at a frequency of 11 Hz and at a scan rate of 2°C/min over the temperature range of 30–220°C. A fixed tension level of 0.25 gf/d was maintained on the sample during the test.

DSC

Thermal traces of the filament samples were conducted on a Perkin-Elmer series 7 thermal analysis differential scanning calorimeter interfaced to a Perkin–Elmer model 7700 professional computer. Samples weighing approximately 8 mg were scanned at 40°C/min over the range from 50 to 300°C. Filaments were cut such that small segments could be laid flat in the DSC sample pan. This method of sample preparation assured that no portion of the fiber length was constrained during the scanning process. All scans were normalized to eliminate differences due to sample weight.

Wide-Angle (WAXS) and Small-Angle X-Ray Scattering (SAXS)

A Siemens type-F X-ray diffractometer equipped with a nickel-filtered CuK_α radiation source and an evacuated camera (designed by W. O. Statton) was used to generate wide-angle flat plate photographs. The camera was set up using a pinhole collimator of 0.25 mm diameter and a sample to film distance of 8 cm.

The WAXS analysis was performed by the Allied-Signal Fibers Division using a Philips APD 1700 diffraction system in transmission mode with a CuK_α radiation source. The samples were mounted as a bundle of parallel filaments. Equatorial and meridional intensity scans were collected and profile fit using the appropriate number of Pearson VII functions.[12,13] The apparent lateral (010, 100) and longitudinal ($\bar{1}05$) crystallite dimensions were then calculated using the Scherrer equation,[14]

$$L_{hkl} = \frac{K\lambda}{\beta \cos \theta} \tag{5}$$

where β is the peak halfwidth, K is taken to be unity, λ is the radiation wavelength, and θ is the Bragg angle. The crystallite orientation factor was determined using the Hermans function,

$$f_c = (3\langle \cos^2 \phi \rangle - 1)/2 \tag{6}$$

where ϕ was taken as the full width at half maximum of the profile fit $\bar{1}05$ reflection generated from an azimuthal scan. The amorphous orientation factor was then calculated using the expression derived through the application of a simple two phase model as described by Stein and Norris,[15] which relates the overall measured filament birefringence (Δn) to the contributions from both the crystalline and amorphous phases:

$$\Delta n = f_c V_c \Delta n_c + f_a (1 - V_c) \Delta n_a \tag{7}$$

where Δn_c and Δn_a represent the intrinsic birefringences of perfectly crystalline and amorphous PET, whose values were taken as 0.22 and 0.275,[16] respectively.

The SAXS analysis was performed at the Oak Ridge National Laboratory using a rotating anode CuK_α X-ray source, pinhole collimation (2 mm diameter at the sample), a sample to detector distance of 5 m, and a 2-dimensional position-sensitive detector with dimensions of 20 × 20 cm. The angular dimensions associated with the isointensity contour plots are in units of momentum transfer, Q, which is defined as

$$Q = (4\pi/\lambda)\sin(\theta_{\text{scat}}/2) \tag{8}$$

The long period spacing (LPS) of the repeat lamellar structure was then calculated as

$$\text{LPS} = 2\pi/Q \tag{9}$$

where θ in eq. (8) is taken as the angular separation of the quadrant spots or meridional streaks in a direction parallel to the fiber axis.

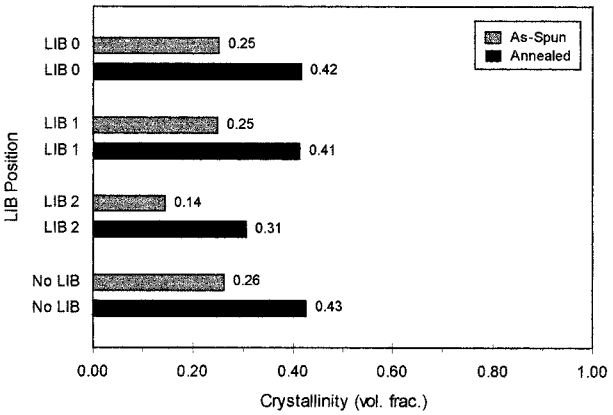

Figure 2 Volume fraction crystallinity as a function of LIB position for as-spun and annealed PET filaments produced using a liquid isothermal bath modified spinning process.

RESULTS AND DISCUSSION

Crystallinity and Birefringence of As-Spun and Annealed Filaments

Figure 2 shows the volume fraction crystallinity as a function of LIB position for the as-spun and annealed filaments. The LIB 0, LIB 1, and no LIB as-spun samples all have essentially equivalent values of crystallinity. The consistency among these three samples persisted through the annealing process, and each of these samples experienced a comparable increase in crystallinity. As for the LIB 2 sample, the crystallization process appears to have been stifled to a certain degree in both the as-spun and annealed filaments. Figure 3 shows birefringence as a function of LIB position for the as-spun and annealed filaments. Birefringence of the as-spun LIB samples increased from 0.115 for the position closest to the spinneret (LIB 0) to 0.189 for the position most distant from the spinneret (LIB 2). Birefringence of the as-spun no LIB sample was the lowest of all at 0.091, which is well within the range expected for an unperturbed spinning process operating at 4000 m/min. Subsequent annealing resulted in a significant increase in birefringence for the no LIB sample, while all of the LIB samples (0–2) experienced little to no change in birefringence as a result of the annealing process.

Two prominent features of the as-spun LIB filaments were identified. The first was the suppression of crystallization that occurs when the LIB is operated at a position relatively distant from the spinneret (LIB 2). As described in previous studies,[4–8] use of the LIB forces extremely high threadline tensions to develop as a result of the drag experienced at the filament–liquid interface. One previous interpretation of this diminished crystallization phenomenon was that such a high level of threadline tension was experienced within the bath that the growth of crystallites was hindered due to restricted motion of the neighboring chain segments.[4,5] Another possible contributing factor, which has yet to be considered, centers around the behavior of the threadline above the bath. When the LIB is operated at a position relatively distant from the spinneret, the threadline tension above the bath drops dramatically and the threadline temperature actually drops below the glass transition temperature before entering the bath. Hence, a precursor structure of sorts has already been formed, which is most certainly poorly oriented and nearly completely amorphous. From this perspective, the limited crystallization that develops may be considered to be a consequence of the poor orientation that the developing threadline possesses as it makes its virgin pass through the temperature range known to facilitate crystallization during the cooling process. The drawing and reheating that undoubtedly occurs in the bath is not quite able to compensate for the poorly developed structure of the nearly solidified filament that enters the bath. As for the second prominent feature, this is clearly the unprecedented high birefringence values achieved in the as-spun filaments through use of the LIB process. In fact, the birefringence values of the as-spun filaments produced using LIB positions 1 and 2 rival those of PET filaments spun at low speed and subsequently

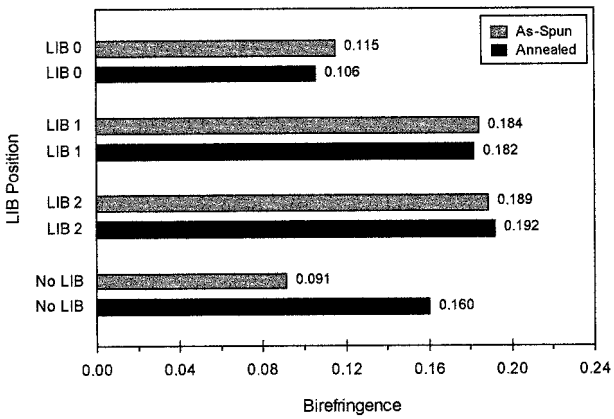

Figure 3 Birefringence as a function of LIB position for as-spun and annealed PET filaments produced using a liquid isothermal bath modified spinning process.

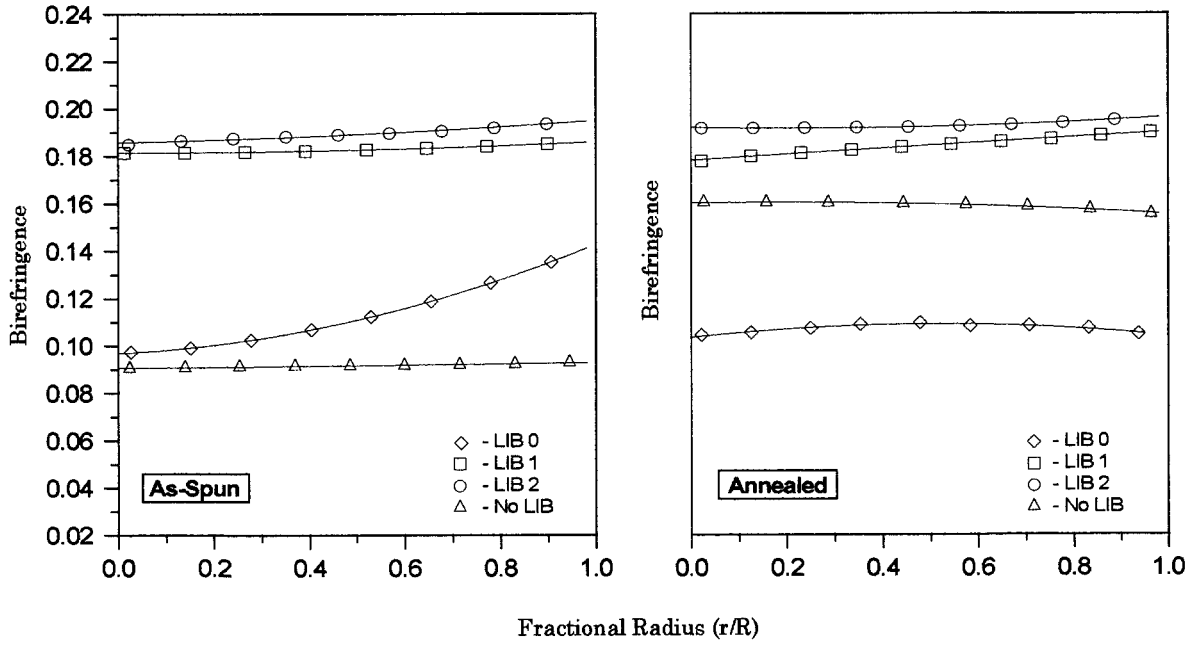

Figure 4 Radial birefringence profiles of as-spun and annealed PET filaments produced using a liquid isothermal bath modified spinning process.

drawn up to 4 times their original length. Previous studies showed that the level of orientation present in the as-spun filament is directly related to the stress experienced in the developing threadline.[3,17,18] As described above, the drag that occurs at the filament–liquid interface forces extremely high threadline stresses to develop. Hence, the established relationship between stress and orientation appears to have been verified in this case as well with new upper limits being demonstrated. Note that the increase in birefringence for the annealed no LIB sample is attributed primarily to yielding that occurred during the annealing process as a result of the pretension imposed by the slight difference in roll speeds.

Figure 4 shows the radial birefringence profiles of the as-spun and annealed filaments for each LIB position, as well as for the unperturbed no LIB condition. Note that the birefringence shown for the center of each filament ($r/R = 0$) may not correspond exactly to the mean birefringence values reported in Figure 3. This is due to the fact that the mean birefringence values actually represent a chord average birefringence across the filament and therefore should not be expected to correspond exactly with the values shown here for the center of each filament. As shown in Figure 4, the LIB 1, LIB 2, and no LIB samples all possess very flat profiles in both the as-spun and annealed filaments. In light of the well-known tendency for radially differentiated structures to develop during high-speed spinning, the ability to generate such highly oriented, radially uniform as-spun structures, such as those present in the LIB 1 and LIB 2 samples, is considered to be one of the most attractive features of this LIB technology. As for the LIB 0 sample, a modest sheath-core type of structure is present in the as-spun filament. The development of this sheath-core structure is considered to be at least partially the result of the rapid quench that occurs as the presumably higher temperature filament first enters the liquid, thereby forcing an even greater temperature gradient across the filament for a brief instant prior to thermal equilibration. As for the annealed LIB 0 sample, the minor drop in sheath orientation is likely due to relaxation that occurred as the filament was exposed to the elevated annealing temperature. The fact that only the LIB 0 sample experienced this decline in sheath orientation could be an indication that some minor slippage occurred during the annealing of this sample. The significant increase in birefringence of the annealed no LIB sample is attributed primarily to yielding that occurred during annealing as a result of the imposed pretension.

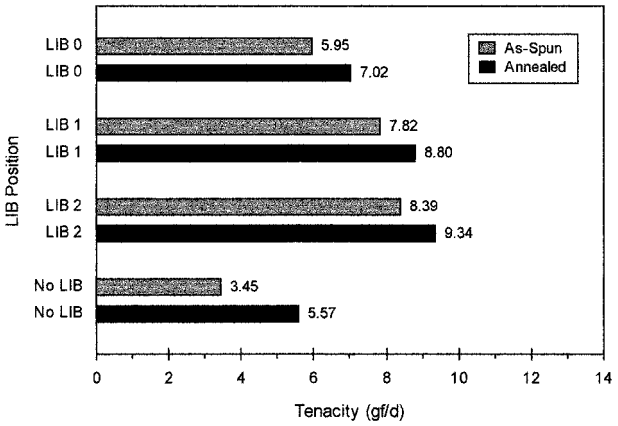

Figure 5 Tenacity as a function of LIB position for as-spun and annealed PET filaments produced using a liquid isothermal bath modified spinning process.

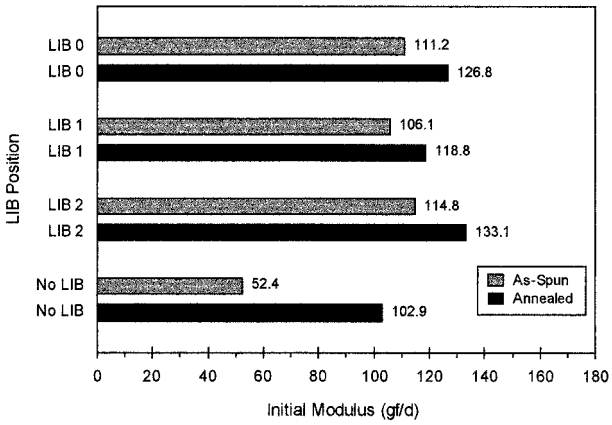

Figure 7 Initial modulus as a function of LIB position for as-spun and annealed PET filaments produced using a liquid isothermal bath modified spinning process.

Tensile Properties of As-Spun and Annealed Filaments

Figure 5 shows tenacity as a function of LIB position for the as-spun and annealed filaments. The as-spun no LIB filament had the lowest tenacity of all of the samples at 3.45 gf/d. Use of the LIB resulted in dramatic increases in the as-spun tenacities, and values ranged from 5.95 gf/d for LIB position 0 to 8.39 gf/d for LIB position 2. In every case the annealing process increased the tenacity, and the largest percentage increase was observed in the no LIB sample. Figure 6 shows elongation to break as a function of LIB position for the as-spun and annealed filaments. The as-spun no LIB filament had the highest elongation of all of the samples at 66.9%. The as-spun LIB filaments possessed elongations ranging from 15.4% for LIB position 0 to 10.3% for LIB position 2. Subsequent annealing again resulted in the most significant change, a decrease in this case, in the elongation to break for the no LIB sample, followed by a somewhat smaller percentage decrease for the LIB 0 sample. As for the LIB 1 and LIB 2 samples, no significant change in elongation to break was observed upon annealing. Figure 7 shows the initial modulus as a function of LIB position for the as-spun and annealed filaments. The as-spun no LIB filament had a modulus of 52.4 gf/d, which again represents the poorest performance among all of the samples. The as-spun LIB filaments, while showing little response to varying LIB positions, all had modulus values that more than doubled the value observed for the as-spun no LIB filament. As for changes incurred during the annealing process, the no LIB sample experienced the greatest increase in modulus by far with a value of 102.9 gf/d achieved. The annealed LIB filaments all experienced much more moderate increases in modulus with values ranging from 118.8 to 133.1 gf/d. Figure 8 shows the SAR as a function of LIB position for the as-spun and annealed filaments. As described previously, this quantity represents the magnitude of the deviation from linearity in stress–strain behavior that occurs just beyond the yield point. As in all of the tensile properties considered, the as-spun no LIB filament also possessed the lowest SAR value, which indicates its extremely poor resistance to further nonrecoverable deformation

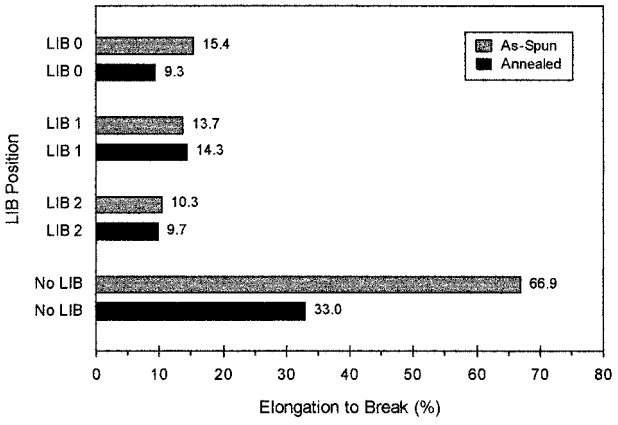

Figure 6 Elongation to break as a function of LIB position for as-spun and annealed PET filaments produced using a liquid isothermal bath modified spinning process.

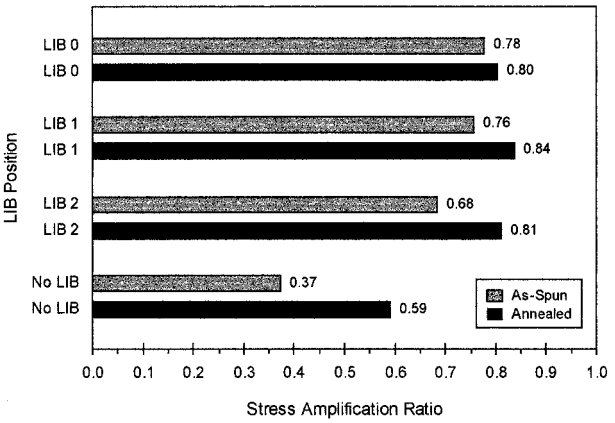

Figure 8 Stress amplification ratio as a function of LIB position for as-spun and annealed PET filaments produced using a liquid isothermal bath modified spinning process.

when strained beyond the yield point. Even after annealing, the no LIB sample still displayed yield behavior considered unacceptable for direct use in any type of reinforcement application. Although all of the as-spun LIB samples had yield resistance superior to the no LIB sample, the SAR value for the LIB 2 sample was considerably lower than either the LIB0 of LIB1 samples. This deficiency is likely the result of the low level of crystallinity present in the as-spun LIB2 sample.

The tensile properties are unquestionably the most important and most often characterized feature of polymeric filaments. In a production environment, the tracking of these quantities is used as a means of monitoring quality. In a research environment, the response and balance of these quantities are used as a means of gauging the effectiveness of new process modifications. The as-spun filament tensile properties in the present study varied over an exceptionally wide range, especially when considering that the take-up speed remained fixed at 4000 m/min during the collection of all samples. The general increase in tensile properties observed for the LIB filaments was attributed to the greater level of orientation and the increased number of load bearing chains. In addition, a preceding study, which employed infrared spectroscopy to investigate the conformation of molecular chains at the surface of crystallites present in a very similar set of filament samples, found evidence that is considered supportive of the hypothesis that these uniquely produced LIB filaments possess a greater content of extended chain type crystals, as well as an enhanced level of molecular connectivity among the amorphous and crystalline phases.[19] Examination of the annealed LIB filament properties showed that this particular type of posttreatment is capable of providing only a moderate increase in tensile performance.

Thermal Analysis of As-Spun and Annealed Filaments

Figure 9 shows boil-off shrinkage and free shrinkage at 177°C as a function of LIB position for the as-spun and annealed filaments. The boil-off shrinkage was lowest in the as-spun LIB 0 sample at 7.8%. The boil-off shrinkages of the as-spun LIB 1, LIB 2, and no LIB samples were all significantly higher with values of 12.9, 12.2 and 15.0%, respectively. All of the annealed samples were subjected to a higher temperature free shrinkage test that was performed in air at 177°C. Clearly, the annealing process improved the dimensional stability of all of the LIB samples, as well as that of the no LIB sample.

The shrinkage propensity of a filament, or fiber, is often attributed to the balance between orientation and crystallinity[20] where high levels of orientation induce large shrinkages, while high levels of crystallinity exhibit an opposite effect and almost always result in lower shrinkages. As described in the discussion of Figures 2 and 3, the as-spun samples characterized in the present study possess a wide range of orientations while maintaining an essentially constant level of crys-

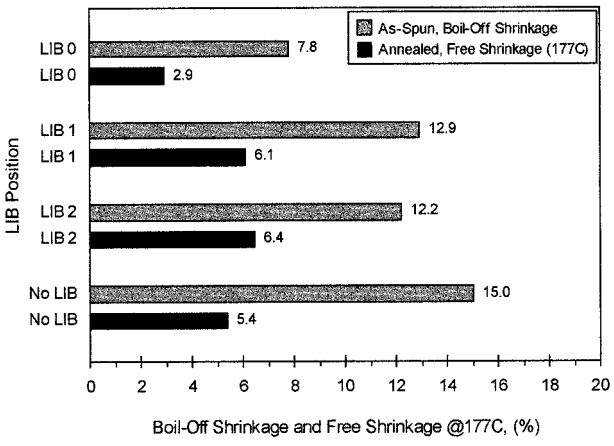

Figure 9 Boil-off shrinkage and free shrinkage at 177°C as a function of LIB position for as-spun and annealed PET filaments produced using a liquid isothermal bath modified spinning process.

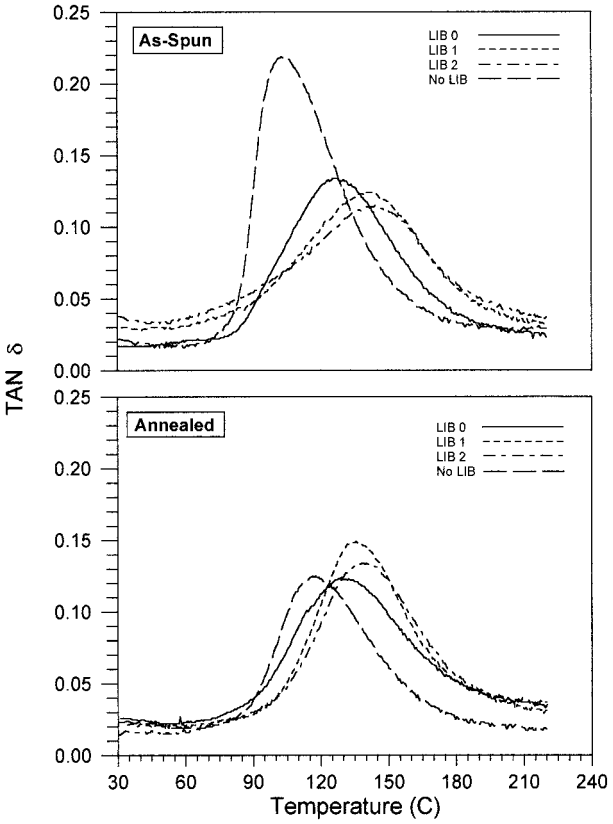

Figure 10 Loss tangent as a function of temperature for as-spun and annealed PET filaments produced using a liquid isothermal bath modified spinning process.

tallinity. This situation should allow the lone effect of orientation to be more clearly established. However, using the birefringence data presented in Figure 3 as a crude approximation of the amorphous orientation, comparison with the boil-off shrinkage data shown in Figure 9 indicates that the as-spun LIB samples do not conform with the expected shrinkage behavior. In accord with the previous findings of Zhou et al.,[19] the lessened shrinkage propensity of the highly oriented as-spun LIB filaments is attributed to their novel crystalline morphology, which will be discussed in more detail in the next section. The consistently improved dimensional stability observed for each of the annealed samples is attributed to the significant increase in the overall level of crystallinity resulting from the high temperature posttreatment.

Figure 10 shows the loss tangent as a function of temperature for the as-spun and annealed filaments. The loss tangent peak of the as-spun LIB samples moved to higher temperature, became smaller in magnitude, and increased in width as the LIB position was moved further from the spinneret. The loss tangent peak of the as-spun no LIB sample occurred at a much lower temperature and was nearly double in magnitude when compared to any of the as-spun LIB samples. Annealing of the LIB samples caused the loss tangent peak temperature and magnitude to change very little, while the width of each peak was consistently narrowed. Annealing of the no LIB sample resulted in a moderate increase of the loss tangent peak temperature and a large reduction in peak magnitude and width.

The dynamic loss tangent is defined as the ratio between the loss and storage moduli and represents the fraction of energy lost per cycle due to viscous dissipation. The location of the loss tangent peak indicates the initiation of micro-Brownian motion of molecular chains within the amorphous regions and is usually referred to as the α or primary transition. Among the most prominent interpretations of the α transition are those of Murayama,[21] Kamide et al.,[22,23] and Takayanagi and Matsuo.[24,25] These interpretations suggest that the behavior of the α transition can be used to make strong inferences in regard to the relative mobility and/or packing density associated with the amorphous regions. When the basic relationships derived through each of these interpretations are applied to the loss tangent data presented here, the relative differences in amorphous mobility and packing density become more easily gauged and articulated. The higher transition temperatures of the as-spun LIB samples are indicative of a less mobile and/or more densely packed amorphous phase. The corresponding reduction in peak magnitude of these same transitions also indicate a decrease in the amount of amorphous material considered to be relatively mobile, while the increased peak width indicates the presence of a broader distribution with regard to segment mobility and/or packing density of the amorphous phase. Note that annealing of the no LIB sample produced the most dramatic changes; however, its amorphous phase remained more mobile and/or less densely packed than in any of the annealed LIB samples. As for the general narrowing that occurred in all of the transition peaks upon annealing, this may be due to the development of better defined boundaries and a clearer distinction between the crystalline and amorphous phases.

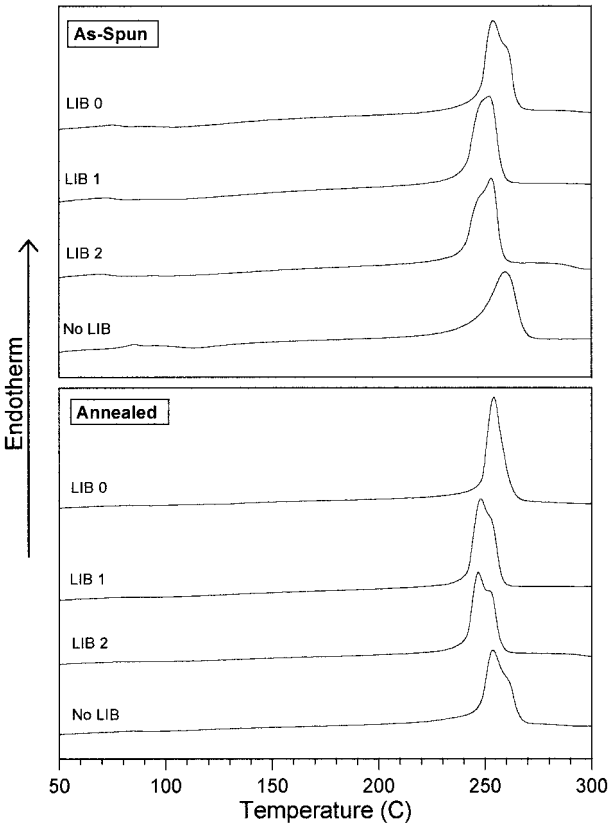

Figure 11 DSC traces of as-spun and annealed PET filaments produced using a liquid isothermal bath modified spinning process (scan rate = 40°C/min).

Figure 11 shows the DSC traces of the as-spun and annealed filaments. All of the as-spun LIB samples display very subtle glass transitions, no strong evidence of a crystallization exotherm, and melting endotherms that occur at relatively low temperature. These melting endotherms also appear to consist of dual overlapping peaks, and the balance in magnitude between each set of overlapping peaks varies with LIB position. The as-spun no LIB sample has a slightly more pronounced glass transition, indication of a very minor crystallization exotherm, and the highest temperature melting endotherm that in this case appears to consist of only a single peak. Annealing of the LIB samples resulted in even more subdued glass transitions and again, as would be expected from a previously annealed material, no indication of a crystallization exotherm. As for the melting endotherms of these annealed LIB samples, the balance in magnitude between the apparent dual peaks shifted, and the lower temperature portion of each set of peaks became larger. Upon annealing, the lower temperature peak of the LIB 0 sample grew to the extent that the higher temperature peak could no longer be distinguished. Although annealing of the LIB 1 and 2 samples also resulted in an increase in magnitude of the lower temperature peak, the increase was not of such magnitude that the higher temperature peak could no longer be distinguished. Finally, annealing of the no LIB sample resulted in the development of a large and distinct lower temperature peak, thus giving rise to a dual peak melting endotherm that appears roughly similar in shape to the melting endotherms of the annealed LIB 1 and 2 samples, but occurs at a slightly higher temperature.

The most prominent features of a ASC trace are the temperature and magnitude of the glass transition, the crystallization exotherm, and the melting endotherm. In accord with the interpretation of Wunderlich et al.,[26,27] the virtual nonexistence of a glass transition suggests that all of the as-spun LIB samples possess a relatively rigid amorphous phase. In light of the established propensity of the as-spun LIB filaments to crystallize when heated, the lack of a detectable crystallization exotherm in the DSC traces is likely due to the relatively small change in entropy associated with the transformation from a highly oriented amorphous phase to a perfectly ordered crystalline phase. The dual peak nature of the as-spun LIB filament melting endotherms was observed previously in PET, but only in filaments that had been subjected to some level of high temperature posttreatment. However, in agreement with the results of a previous study[19] and the fact that the filaments have yet to be subjected to any type of traditional posttreatment, it could be hypothesized that each of the lower temperature peaks represents a contribution from less perfected crystallites and each of the higher temperature peaks, especially for the LIB 0 case, represents a contribution from crystallites of greater perfection that possess a larger portion of extended chain segments. Upon further comparison of the glass transition magnitude and the peak melting temperature, it appears that the as-spun no LIB filament possesses a more mobile amorphous phase and crystallites of relatively larger dimension, respectively, than any of the as-spun LIB filaments. The lack of a distinct glass transition and crystallization exotherm in any of the annealed filaments suggests that they all possess a relatively rigid amorphous phase and well-developed crystalline

structure. However, it should be noted that the analysis and interpretation of DSC traces is not considered to be one of the more powerful tools in the study of amorphous phase fine structure. As for the melting endotherms of the annealed samples, the consistent increase in magnitude of the lower temperature component of the dual peaks is attributed to an increase in the content of less perfected crystalline material, such as some type of overgrowth on existing crystallites that occurs during the annealing process.

X-Ray Analysis of As-Spun and Annealed Filaments

Figure 12 shows the WAXS patterns of the as-spun and annealed filaments. The as-spun LIB 0 filament pattern exhibits a discernible halo and intense diffuse scattering along the equator, as well as some reasonably well-defined off-equator reflections or layer lines. The as-spun LIB 1 and LIB 2 filaments both yield patterns that are dominated by intense, yet still relatively diffuse, scattering along the equator. The as-spun no LIB filament pattern displays a weak uniformly distributed halo and sharp reflections of moderate intensity. All of the annealed filament patterns display relatively sharper equatorial reflections, as well as the emergence of considerably stronger off-equator reflections, both of which are indicative of a more well-developed crystalline structure. The diffuse equatorial scattering that is clearly present to a varying extent in all of the LIB filament patterns could potentially result from a combination of factors, such as the concentration of scattering from an oriented amorphous phase,[28] poorly oriented crystallites, and/or an overexposure of the film. Hence, a more exact investigation of the crystalline structure was also performed via the detailed analysis of various crystallite reflections. The results from this analysis yielded lateral (010, 100) and longitudinal ($\bar{1}05$) crystallite dimensions and a crystallite orientation factor (f_c); these values are presented in Table I. Also included in Table I are values for the amorphous orientation factor (f_a) that were arrived at through the application of a simple two phase model. The following discussion utilizes the WAXS patterns as a qualitative tool for identifying general features and then refers to the experimentally derived crystallite dimensions and orientation factors when clarification and greater detail are required.

The primary features of interest in WAXS patterns are considered to be the presence, or lack thereof, of scattering from both crystalline and amorphous components and the shape and magnitude of the corresponding intensity distributions from each of these components. The equatorial reflections observed in all of the as-spun LIB filament patterns appear much broader in comparison to those present in the as-spun no LIB filament pattern. This suggests that the lateral crystallite dimensions are relatively smaller in all of the as-spun LIB filaments, which is corroborated by the derived dimensions listed in Table I. A trend among the lateral crystallite dimensions within the series of as-spun LIB samples (0–2) also emerged; the lateral dimensions continually decreased as the LIB was operated at a position more distant from the spinneret. The longitudinal (axial) dimension of the crystallites was determined using a meridional intensity scan of the $\bar{1}05$ reflection, which lies at a Bragg angle ($\cong 43°$) beyond that covered by the scattering patterns. This longitudinal dimension was also found to respond in much the same manner as the lateral dimensions. While the orientation of the crystallites can be roughly estimated by the circumferential length of the reflection arcs, an accurate appraisal of the true reflection arc length via photographic means can easily be distorted by such previously noted factors as overlap scattering from an oriented amorphous phase and/or overexposure of the film. Focusing on the more rigorously derived crystallite orientation factor values shown in Table I indicates that all of the as-spun LIB samples (0–2) and the as-spun no LIB sample possess crystallites that are highly oriented with respect to the filament axis. In accord with eq. (7), the birefringence, percent crystallinity, and crystallite orientation factor data were combined to yield an amorphous orientation factor for each of these samples. Clearly the level of amorphous orientation present in the as-spun LIB filaments ($f_a = 0.298–0.673$) is much greater than in the as-spun no LIB filament ($f_a = 0.174$). Recalling the comparable levels of crystallinity and the significant differences that exist among crystallite dimensions indicates the existence of an as-spun LIB filament morphology that is considered unique by virtue of the presumably greater number of smaller and highly oriented crystallites that are dispersed within a significantly more oriented amorphous phase. As described in a previous study,[19] one potential benefit of such a structure is the likelihood of enhanced molecular connectivity

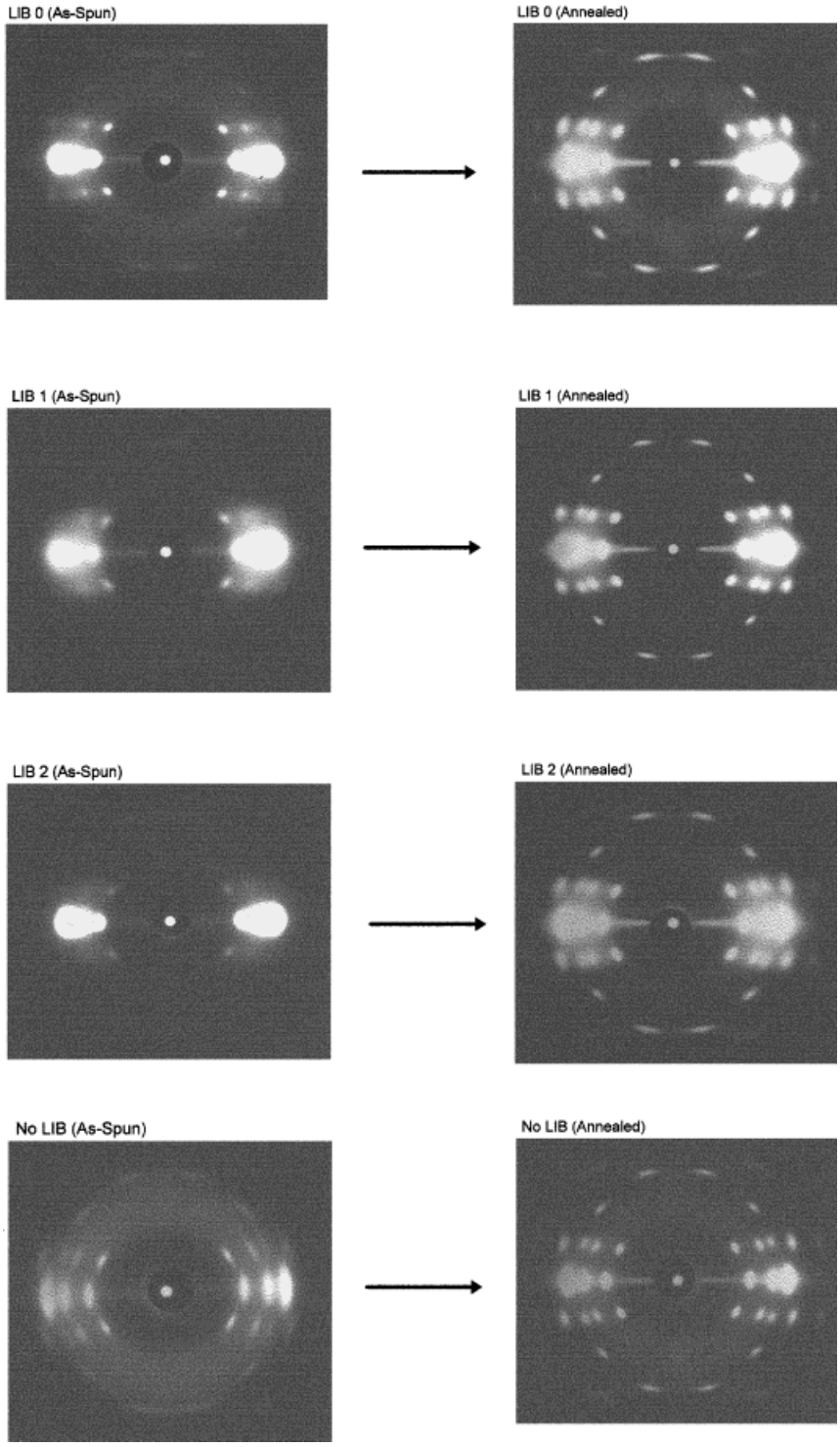

Figure 12 WAXS patterns of as-spun and annealed PET filaments produced using a liquid isothermal bath modified spinning process.

Table I Crystallite Dimensions, Orientation Factors, and Long Period Spacings (LPS) of As-Spun and Annealed PET Filaments Produced Using Liquid Isothermal Bath Modified Spinning Process

Sample Identification	010 (Å)	100 (Å)	$\bar{1}05$ (Å)	f_c	f_a	LPS (Å)
LIB 0 (as spun)	39	42	74	0.972	0.298	—
LIB 1 (as spun)	36	29	70	0.976	0.632	—
LIB 2 (as spun)	33	24	68	0.971	0.673	—
No LIB (as spun)	53	53	91	0.972	0.174	—
LIB 0 (annealed)	76	54	98	0.985	0.094	167
LIB 1 (annealed)	64	48	93	0.986	0.574	162
LIB 2 (annealed)	64	48	90	0.986	0.657	167
No LIB (annealed)	83	64	98	0.976	0.432	176

among the amorphous and crystalline regions. As shown in Figure 12, the process of annealing sharpened all of the already present reflections, while also bringing out the off-equator reflections that were either very weak or nonexistent. However, the equatorial reflections (arcs) present in all of the annealed LIB patterns appear to remain slightly broader than those present in the annealed no LIB pattern. As described previously, these broader equatorial reflections imply that crystallites of smaller lateral dimension persist even in the annealed LIB filaments, which is again confirmed by the intensity scan derived crystallite dimensions shown in Table I. In all of the LIB samples the crystallite growth that occurred during the annealing process resulted in a concurrent drop in amorphous orientation. The unanticipated higher level of amorphous orientation in the annealed no LIB sample was considered to be an artifact and the direct result of inadvertent strain imposed during the annealing process. Finally, the crystallite dimensions and orientation factors derived from the WAXS are considered to be in agreement with previous findings[4–7] which showed that use of the LIB resulted in a significant restriction to the growth of crystallites during the spinning process. The rationale for this behavior remains unchanged: the high level of threadline stress that develops from the drag experienced at the filament–liquid interface forces the constituent chains to be strained to such an extent that the chain segment mobility required for crystallite growth becomes significantly hindered. The amorphous phase of the as-spun LIB filaments that envelop these smaller crystallites was identified as being significantly more oriented, as well as more rigid. This increased rigidness of the as-spun LIB filament amorphous phase may, in a manner similar to that experienced during the initial spinning process, continue to limit chain segment mobility and thereby be responsible for the smaller lateral crystallite dimensions that persist even in the annealed LIB filaments.

Figure 13 shows the SAXS patterns of the as-spun and annealed filaments. The as-spun LIB 0 filament produces a pattern in which scattering occurs in all directions, although the scattering that occurs in the equatorial direction is slightly elongated. The as-spun LIB 1 filament yields a pattern in which the scattering is now concentrated along the equator in a much more elongated fashion. The as-spun LIB 2 filament generates a scattering pattern similar to that of the LIB 1 filament; however, the equatorial scattering now appears to have become more radially diffuse as the scattering angle increases or, as shown in Figure 13, as the momentum transfer function (Q) deviates from zero. The as-spun no LIB filament produces the well documented X or cross-shaped pattern. Annealing of each of these as-spun filaments resulted in an increase of the scattering intensity and the development of well-defined coherent scattering peaks centered along the meridian. These peaks are commonly described with regard to their general shape and the number of plateau regions, which typically results in patterns being classified as two point, four point, or bar shaped. Following this nomenclature convention, the annealed LIB 0 filament produced a bar-shaped streak with its long direction oriented perpendicular to the filament axis. The annealed LIB 1 and LIB 2 filaments both produced even more elongated bar-shaped streaks, with the two streaks present in the LIB 1 filament pattern having clearly separated to yield a four-point pat-

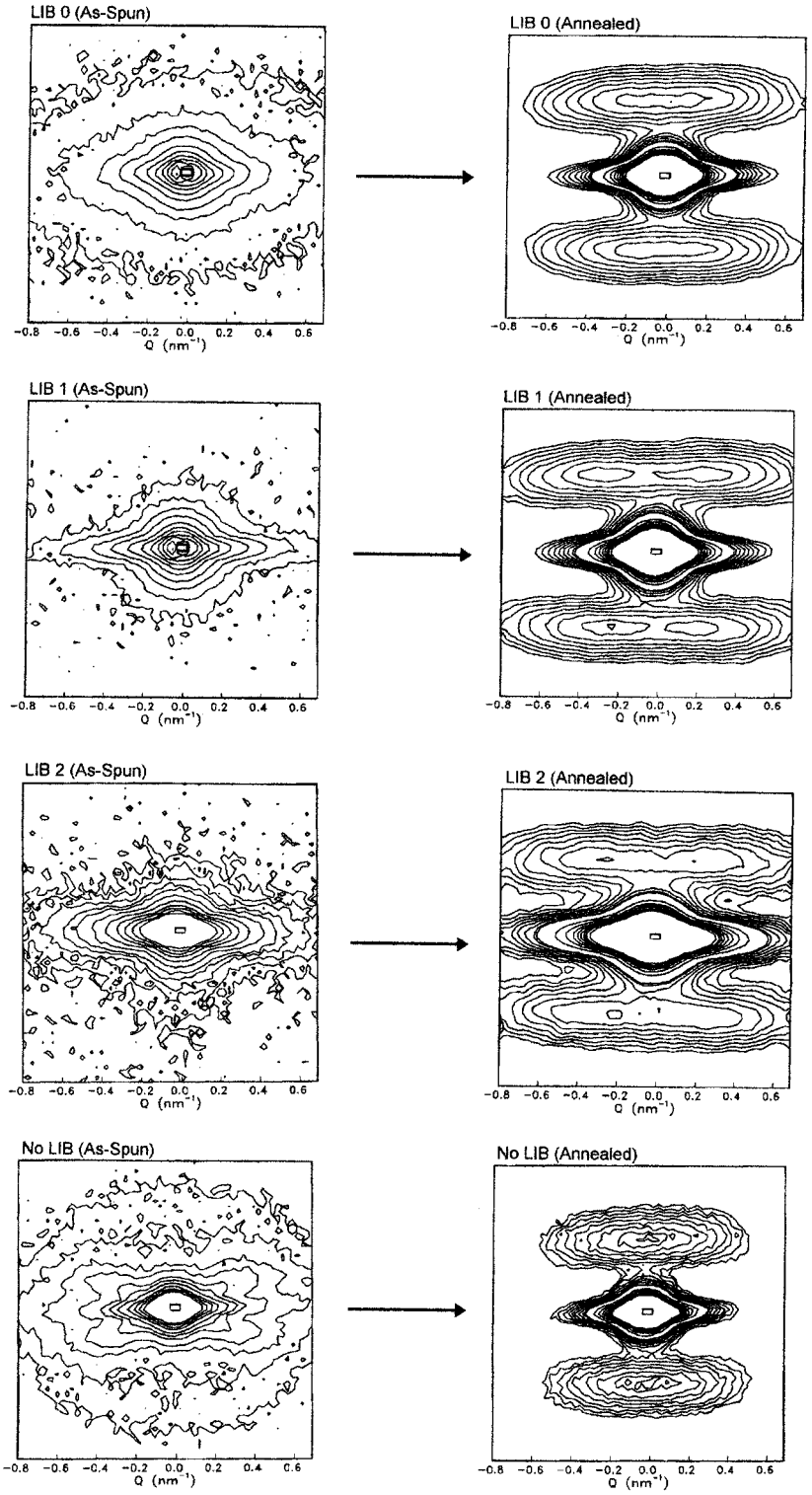

Figure 13 SAXS patterns in isointensity contour plot format of as-spun and annealed PET filaments produced using a liquid isothermal bath modified spinning process.

tern. As for the annealed no LIB filament, this sample had a much sharper and weakly elongated meridional streak. The determination of a longitudinal LPS requires well-defined maxima along the meridional direction; hence, this quantity was determined only for the annealed filaments. The values for these are shown in Table I. Note, the apparent ring, or flat spot, centered around the beam stop in all of the annealed filament patterns is an artifact of the scaling of contour lines, which were chosen to accentuate the lobes. The missing portion of the data show only a steady increase until a Q value of about 0.05 nm^{-1}, at which point the beam stop is reached.

The scattering of X rays at small angles is attributed to fluctuations in electron density. Therefore, the uniform distribution of scattering that occurs in the pattern of the as-spun LIB 0 filament suggests that the electron density fluctuates in a 2-dimensional manner or that it fluctuates across the filament axis, as well as along its length. This more or less random fluctuation in electron density indicates that the relatively smaller, yet highly oriented, crystallites present in the as-spun LIB 0 filament are randomly located along both the longitudinal and lateral directions, which again is in good agreement with the hypothesized uniform distribution of crystallites for a filament of this type as put forth in a related previous study.[19] The pattern of the as-spun LIB 1 filament exhibits scattering that is much more concentrated along the equator. This concentration of incoherent scattering along the equator indicates that the source of the electron density fluctuation has become more oriented with respect to the filament axis; however, as also observed in the previous case, the fluctuation does not occur in any type of periodic fashion. The pattern of the as-spun LIB 2 filament appears somewhat similar to that of the as-spun LIB 1 filament, except for the tendency of the equatorial scattering to fan out as the scattering angle increases. According to Harburn et al.,[29] this fanning out of the equatorial streak is due to misorientation of the source of the scattering. However, the high birefringence previously reported for this sample suggests that the misorientation of the scattering source is more likely related to alignment difficulties associated with sample preparation. All of the as-spun LIB filament patterns lack any indication of periodicity along the direction of the filament axis, hence the small crystallites that are believed to be present have yet to establish themselves in any regular order as would be expected if a fibrillar structure were already present. While the presence of strong equatorial scattering has also been attributed to the presence of elongated and preferentially oriented microvoids, the onset of microvoid formation is usually associated with the use of much higher take-up speeds where a concurrent decline in tensile properties is also observed. Because the tensile properties of both the as-spun LIB 1 and LIB 2 filaments are clearly superior to any such filaments produced at ultrahigh take-up speeds, the source of the electron density fluctuation that gives rise to the incoherent equatorial scattering observed in the patterns of these filaments is attributed in greater likelihood to the emerging cylindrical symmetry of this highly oriented transitional structure. As a general comment regarding equatorial scattering at small angles, the numerous possibilities that could force such scattering to occur dictates that the interpretation cannot be considered unambiguous.[29–31] The pattern of the as-spun no LIB filament is most differentiated from the as-spun LIB filament patterns by the presence of an X or cross-shaped scattering pattern. This nonmeridional radial-type scattering suggests the possibility of a large longitudinal periodicity buried by beam stop scattering and/or an inclination with respect to the filament axis of the source of the electron density fluctuation.[32] This type of scattering has also been associated with crystallites that exist in a form that more closely resembles a lamellae structure than a fibrillar structure.[33] The annealing of each of these as-spun filaments has consistently resulted in a structure that produces coherent scattering in the meridional direction. This coherent scattering manifests itself as well-defined maxima that are typically referred to as lobes. The interpretation of this coherent meridional scattering is undisputedly the result of a regular or periodic fluctuation in electron density along the direction of the filament axis. The linear dimension of this LPS is given in Table I for each of the annealed samples. The LPSs of all of the annealed LIB filaments vary over a narrow range from 162 to 167 Å. As for the slightly larger LPS of the annealed no LIB filament, inadvertent strain incurred during the annealing of this sample gravely limits the appropriateness of any explanation based on as-spun structural differences. Additional qualitative information regarding the relative size and apparent shape of the crystallites can also be derived from the shape of the lobes. The uniform

width of each lobe in the direction of the filament axis suggests that all of the annealed filaments possess crystallites that are of comparable longitudinal dimension. As for the width of each lobe in the direction transverse to the filament axis, all the annealed LIB filaments produce patterns in which this dimension of the lobes is elongated or broad in comparison to that observed in the annealed no LIB filament. This feature suggests that the annealed LIB filaments all possess crystallites that are relatively narrower in the direction transverse or perpendicular to the filament axis. However, it must also be noted that a lateral dimension derived via this approach has the potential of being confounded by the broadening of these lobes that can occur as the result of an apparent skewed, or tilted, crystallite surface. Harburn et al.[29] also suggested that broadening of the meridional layer lines could be the result of a more gradual transition in the modulation of electron density along this lateral direction. As these meridional streaks broaden, they will sometimes both split into two separate peaks that give rise to the so-called four-point pattern. The annealed LIB 1 filament produced the only clearly distinguishable four-point pattern. The four-point pattern is usually associated with one of two possible structures. The first of these is a structure in which the crystallites, and hence the constituent molecular chains, are both tilted with respect to the filament axis. The second of these is a structure in which only the apparent face or surface of the crystal is slanted, while the constituent molecular chains remain well oriented and relatively parallel to the filament axis. In light of the high birefringence and high degree of crystallite orientation known to exist, the resulting four-point SAXS pattern of the annealed LIB 1 filament is considered more likely due to the presence of the latter of these two possible structures. Regardless of the varying characteristics of the meridional streaks, all of the annealed filament patterns indicate the presence of long-range periodicity, which is attributed to the longitudinal arrangement of alternating crystalline and amorphous regions.

SUMMARY AND CONCLUSIONS

The unique implementation of an LIB into a melt spinning threadline allowed for previous limits in as-spun orientation and tensile properties to be well surpassed. The large increase in birefringence, while maintaining either an equivalent or lesser degree of crystallinity, indicates that a highly oriented amorphous phase was achieved in the as-spun LIB 1 and LIB 2 filaments. The uncommonly low percent crystallinity observed in the as-spun LIB 2 filament suggests that the crystallization process was somehow hindered for this particular LIB setup. A previously hypothesized explanation cites the development of an extremely high level of threadline stress that acts to dramatically increase the overall orientation while also hindering the growth of crystallites by limiting the necessary local mobility of the constituent chains. This previous explanation appears to also agree well with the data gathered in the present study, at least for the LIB position furthest from the spinneret. As for the corresponding annealed LIB filaments, the birefringence remained essentially constant and the crystallinity and tensile properties increased only moderately.

Thermal analysis indicates that the as-spun LIB filaments experience less shrinkage than the as-spun no LIB filament, even though they possess a higher level of amorphous orientation. The relative ranking among shrinkage values observed in the corresponding annealed filaments followed the more expected response with higher amorphous orientation leading to higher shrinkage. The loss tangent temperature dependence indicates that all of the as-spun and annealed LIB filaments possess a more rigid amorphous phase than that present in either the as-spun or annealed no LIB filament and that the extent of rigidness appears to become more profound as the bath is operated at a position more distant from the spinneret. The DSC melting behavior indicates that the melting point of all of the as-spun LIB filaments range from 5° to 10° below that observed for the no LIB filament. It is also interesting to note that the as-spun LIB filaments already possess a melting endotherm that appears to be composed of dual overlapping peaks, while the as-spun no LIB filament melting endotherm is clearly composed of only a single peak. It is believed that the development of the higher temperature dual peak could perhaps be the result of some kind of novel crystallization that takes place within the bath, possibly even associated with the formation of a more extended chain type of crystalline structure. While the melting points of the annealed filaments remained close to the values observed in each of the precursor as-spun filaments, the annealing process consistently re-

sulted in an increase in relative magnitude of the lower temperature peak.

Structural features of both the as-spun and the annealed LIB(0-2) and no LIB filaments were also investigated through the qualitative inspection of WAXS and SAXS patterns, the quantitative evaluation of lateral and longitudinal crystallite dimensions, and the determination of the crystalline and amorphous orientation factors. In all of the as-spun LIB filaments (0–2), the reflections observed in the WAXS patterns indicate the presence of relatively small crystallites, which is corroborated by the more rigorously intensity scan derived crystallite dimensions. The lack of a uniformly distributed amorphous halo in either the as-spun LIB 1 or LIB 2 filament suggests that the amorphous phase present in these filaments is highly oriented, which is also corroborated by the more rigorously derived amorphous orientation factors. The most prominent feature of the corresponding as-spun filament SAXS patterns is the presence of significant scattering that is elongated along the equatorial direction. The interpretation of this type of equatorial scattering is rarely considered unambiguous. In the present case it is believed to occur as a result of the emerging highly oriented cylindrical symmetry associated with the eventual transformation to a fibrillar structure. WAXS patterns and derived crystallite dimensions also indicate that all of the annealed filaments (LIB 0–2 and no LIB) possess well-developed crystalline structures. However, even after annealing, the LIB filaments appear to have maintained smaller lateral crystallite dimensions. This limited lateral growth of the crystallites is believed to be a consequence of the very rigid nature of the amorphous phase present in the as-spun LIB filaments. The corresponding SAXS patterns indicate that all of the annealed filaments (LIB 0–2 and no LIB) possess well-defined LPSs of comparable dimension, ranging from 162 to 176 Å. The highly elongated (bar shaped) and/or separated (four-point) meridional scattering that occurs in all of the annealed LIB filament patterns are indicative of relatively smaller lateral crystallite dimensions in comparison to the no LIB sample and a tendency for the apparent crystalline–amorphous interfaces to appear skewed or tilted with respect to the filament axis. Note that although the inference regarding the smaller lateral crystallite dimensions taken from the shape of the SAXS meridional lobes has the potential of being confounded by the apparent skew or tilt of the interface, the presence of smaller lateral crystallite dimensions in the LIB filaments was supported by the quantitative analysis of WAXS data.

In conclusion, the ability of the LIB to judiciously control property and structure development in the resulting as-spun filaments was demonstrated. The anticipated strong positional dependence of the effect of the LIB with respect to its location, relative to the point of extrusion, was also demonstrated. The key parameters through which the LIB achieves its profound effect are its ability to significantly increase threadline stress via enhanced drag at the filament–liquid interface and the superior temperature control provided by the much higher thermal conductivity of the liquid, as opposed to air. Finally, it should be evident that the results presented here represent only a small portion of the diverse and novel property–structure balances that the LIB process is capable of generating.

REFERENCES

1. J. A. Cuculo, P. A. Tucker, G. Y. Chen, C. Y. Lin, and J. Denton, *Int. Polym. Processing IV,* **2,** 85 (1989).
2. J. F. Hotter, J. A. Cuculo, and P. A. Tucker, *J. Appl. Polym. Sci.,* **43,** 1511 (1991).
3. G. Y. Chen, J. A. Cuculo, and P. A. Tucker, *J. Appl. Polym. Sci.,* **44,** 447 (1992).
4. G. Y. Chen, Ph.D. dissertation, North Carolina State University, 1990.
5. J. A. Cuculo, P. A. Tucker, and G. Y. Chen, *J. Appl. Polym. Sci., Appl. Polym. Symp.,* **47,** 223 (1991).
6. C. Y. Lin, P. A. Tucker, and J. A. Cuculo, *J. Appl. Polym. Sci.,* **46,** 531 (1992).
7. C. Y. Lin, Ph.D. dissertation, North Carolina State University, 1990.
8. W. Gang, Q. Zhou, J. Y. Chen, J. F. Hotter, P. A. Tucker, and J. A. Cuculo, *J. Appl. Polym. Sci.,* **55,** 1275 (1995).
9. P. B. Rim and C. J. Nelson, *J. Appl. Polym. Sci.,* **42,** 1807 (1991).
10. Z. Wu, Ph.D. dissertation, North Carolina State University, 1993.
11. Z. Wu and H. Davis, *Proc. Roy. Soc.,* to appear.
12. H. M. Heuvel, R. Huisman, and K. C. J. B. Lind, *J. Polym. Sci., Polym. Phys. Ed.,* **14,** 921 (1976).
13. R. Huisman and H. M. Heuvel, *J. Polym. Sci., Polym. Phys. Ed.,* **14,** 941 (1976).
14. P. Scherrer, *Gottingher Nachrichten,* **2,** 98 (1918).
15. R. S. Stein and F. H. Norris, *J. Polym. Sci.,* **21,** 381 (1956).

16. M. Matsui, *Trans. Soc. Rheol.,* **20,** 465 (1976).
17. M. Matsui, in *High-Speed Fiber Spinning,* A. Ziabicki and H. Kawai, Eds., Interscience, New York, 1985, Chap. 5.
18. I. Hamana, M. Matsui, and S. Kato, *Melliand Textilber.,* **50,** 382 (1969).
19. Q. Zhou, G. Wu, P. A. Tucker, and J. A. Cuculo, *J. Polym. Sci., Polym. Phys. Ed.,* **33,** 909 (1995).
20. R. Huisman and H. M. Heuvel, *J. Appl. Polym. Sci.,* **37,** 595 (1989).
21. T. Murayama, *Dynamic Mechanical Analysis of Polymeric Material,* Elsevier, New York, 1978.
22. K. Kamide, T. Kuriki, and S. Manabe, *Polymer,* **18,** 163 (1986).
23. S. Manabe and K. Kamide, *Polym. J.,* **16,** 375 (1984).
24. M. Takayanagi, *Viscoelastic Properties Crystal. Polym.,* **1,** 3 (1963).
25. M. Takayanagi and T. Matsuo, *J. Macromol. Sci., Phys.,* **B1,** 407 (1967).
26. B. Wunderlich, *Thermal Analysis,* Academic Press, New York, 1990, Chap. 6.
27. Y. Fu, W. R. Busing, Y. Jin, K. A. Affholter, and B. Wunderlich, *Makromol. Chem.,* **195,** 803 (1994).
28. K. M. Gupte, H. Motz, and J. M. Schultz, *J. Polym. Sci., Polym. Phys. Ed.,* **21,** 1927 (1983).
29. G. Harburn, J. W. Lewis, and J. O. Warwicker, *Polymer,* **26,** 469 (1985).
30. J. O. Warwicker, *J. Appl. Polym. Sci.,* **19,** 1147 (1975).
31. M. Casey, *Polymer,* **18,** 1219 (1977).
32. J. Shimizu, N. Okui, and T. Kikutani, in *High-Speed Fiber Spinning,* A. Ziabicki and H. Kawai, Eds., Interscience, New York, 1985, Chap. 15.
33. V. I. Gerasimov, Y. V. Genin, A. I. Kitaigorodsky, and D. Y. Tsvankin, *Kolloid-Z. Z. Polym.,* **250,** 518 (1972).